Loss of cone function without degeneration in a novel Gnat2 knock-out mouse

Kaitryn E. Ronning[a], **Gabriel Peinado Allina**[a], **Eric B. Miller**[a], **Robert J. Zawadzki**[b,c,d], **Edward N. Pugh Jr.**[b,c,d], **Rolf Herrmann**[e], **Marie E. Burns**[a,b,d,*]

[a]Center for Neuroscience, University of California Davis, Davis, CA 95616, USA

[b]Department of Cell Biology and Human Anatomy, University of California Davis, Davis, CA 95616, USA

[c]EyePod Small Animal Ocular Imaging Laboratory, University of California Davis, Davis, CA 95616, USA

[d]Department of Ophthalmology & Vision Science, University of California Davis, Davis, CA 95616, USA

[e]Department of Ophthalmology, Medical College of Wisconsin, Milwaukee, WI 53226, USA

Abstract

Rods and cones mediate visual perception over 9 log units of light intensities, with both photoreceptor types contributing to a middle 3-log unit range that comprises most night-time conditions. Rod function in this mesopic range has been difficult to isolate and study *in vivo* because of the paucity of mutants that abolish cone signaling without causing photoreceptor degeneration. Here we describe a novel *Gnat2* knockout mouse line (*Gnat2*$^{-/-}$) ideal for dissecting rod and cone function. In this line, loss of Gnat2 expression abolished cone phototransduction, yet there was no loss of cones, disruption of the photoreceptor mosaic, nor change in general retinal morphology up to at least 9 months of age. Retinal microglia and Müller glia, which are highly sensitive to neuronal pathophysiology, were distributed normally with morphologies indistinguishable between *Gnat2*$^{-/-}$ and wildtype adult mice. ERG recordings demonstrated complete loss of cone-driven a-waves in *Gnat2*$^{-/-}$ mice; comparison to WT controls revealed that rods of both strains continue to function at light intensities exceeding 10^4 photoisomerizations rod^{-1} s^{-1}. We conclude that the *Gnat2*$^{-/-}$ mouse is a preferred model for functional studies of rod pathways in the retina when degeneration could be an experimental confound.

*Corresponding author. Department of Ophthalmology & Vision Science, University of California Davis, Davis, CA 95616, USA. meburns@ucdavis.edu (M.E. Burns).

Declarations of interest

None.

Keywords

G-protein; Photoreceptor; Retina; Phototransduction

1. Introduction

The retinal circuits that relay rod and cone photoreceptor signals to retinal ganglion cells overlap extensively in the mammalian retina. Cones form chemical synapses with cone bipolar cells, which transmit visual signals to retinal ganglion cells (Strettoi et al., 2010). Rods transmit visual information via multiple pathways, all of which involve cone bipolar cells. The primary rod pathway employs chemical synapses between rods and rod bipolar cells, which pass information to A2 amacrine cells, which in turn modulate On- and Off-cone bipolar cells. The secondary rod pathway transmits rod responses via gap junctions directly to cones, which then relay the signals synaptically to cone bipolar cells (Deans et al., 2002). In the less common tertiary rod pathway, rods form chemical synapses directly with cone bipolar cells (Pang et al., 2010). Although convergent pathways from both photoreceptor classes are advantageous for signaling across a wide range of light intensities, such convergence also makes dissecting the functional contributions of rods and cones to the retinal circuitry challenging.

Performing experiments under scotopic or photopic conditions is a useful way to functionally isolate rod and cone signals, but only under those extreme conditions. At intermediate light levels, both rods and cones generate light responses, but the functional consequences of their individual contributions to a combined output are difficult to assess (e.g. Naarendorp et al., 2010). An ideal way to separate the contributions of rod and cone signaling would be to specifically render all the rods or all the cones insensitive to light without disrupting their synaptic connections and partners. Pharmacological manipulations such as superfusion with the metabotropic glutamate receptor agonist, 2-amino-4-phosphonobutyric acid (APB), are commonly used to overwhelm light-driven changes in synaptic release, but such manipulations affect all ON-bipolar cells or all Off-bipolar cells rather than all rod inputs or all cone inputs to the circuitry. Moreover, pharmacologically silencing the cone pathway downstream of cone photoreceptors necessarily eliminates some of the rod input to vision by silencing the secondary rod pathway.

Several mutant mouse lines have been created to genetically silence rod or cone light responses. For example, mice lacking the rod-specific G-protein transducin alpha subunit ($Gnat1^{-/-}$) lack phototransduction signaling downstream of rhodopsin and thus have no rod electrical responses to light, with no detectable concurrent photoreceptor degeneration (Calvert et al., 2000). However, mutants with defects in the cone phototransduction cascade often exhibit morphological abnormalities. One mouse line commonly used to isolate rod function is the $Gnat2^{cpfl3}$ mutant, which contains a single-base pair missense mutation in the gene encoding the cone-specific G-protein transducin alpha subunit, $Gnat2$ (Chang et al., 2006). In these mice, neither $Gnat2$ expression nor cone function is abolished initially, but both decline through adulthood and are finally undetectable by 9 months of

age (Chang et al., 2006). Importantly, rod-driven responses in $Gnat2^{cpfl3}$ mice also decline with age, with clear evidence of photoreceptor degeneration before 27 weeks of age, or approximately 6 months (Chang et al., 2006). More recently, the $Gnat2^{c.518A > G}$ mouse line was found to lack cone function due to an amino acid substitution that results in incorrect protein folding and ultimately a loss of Gnat2 function (Jobling et al., 2013). While the cones of $Gnat2^{c.518A > G}$ mice do not completely degenerate, they exhibit some structural abnormalities as early as 3 months of age, which become more pronounced and lead to Müller cell gliosis as the mice further age. These abnormalities include M-opsin mislocalization, displaced photoreceptor terminals, altered horizontal cell morphology, and altered bipolar cell morphology, suggesting significant disruption to both rod and cone pathways within the circuitry.

Here we describe a novel $Gnat2$ knock-out mouse line ($Gnat2^{-/-}$) that exhibits a complete loss of cone function without retinal degeneration or other noticeable morphological abnormalities. Importantly, rod function in these animals appears to be completely normal throughout adulthood, revealing the upper limit of the mesopic range of rod function, and refining previous estimates for cone thresholds and the magnitude of cone signaling in the mouse.

2. Materials and methods

2.1. Animals

Mice were cared for and handled in accordance with NIH and UC Davis IACUC guidelines. C57BL/6J mice were obtained from the Jackson Laboratory (Sacramento CA). To disrupt $Gnat2$ expression, a 7654 base pair deletion spanning exons 2–9 of the $Gnat2$ gene on chromosome 3 was achieved by inserting a lacZ/Neo cassette using homologous recombination (Fig. 1A). ES cell clones were generated by the UC Davis Mouse Biology Program to yield $Gnat2^{tm1(KOMP)Vlcg}$ during targeting project VG17376, here referred to as $Gnat2^{-/-}$. Vector clones and embryonic stem cells are commercially available from the UC Davis KOMP Repository (Davis, CA). $Gnat2^{-/-}$ ES cells were implanted into 129Sv/J host dams, and subsequently maintained on a C57Bl6/J background for more than 10 generations, with at least 3 rounds of out-and in-breeding $Gnat2$ heterozygotes with particular attention to genotyping for and selecting against the $rd8$ mutation. All mice used in this study lacked the $rd8$ mutation. For specific experiments, heterozygous $Gnat2$ mice were bred to generate both wild-type and knock-out littermates for direct comparisons; because wild-type littermates were phenotypically indistinguishable from C57BL/6J, the two data sets were ultimately pooled for comparisons. In each case, mice of both sexes were used.

2.2. Quantitative real time PCR

Whole retinas were isolated from 3–4-month-old $Gnat2^{-/-}$ and $Gnat2^{+/+}$ littermate control mice. RNA was isolated from whole retinas using the RNeasy Plus Mini Kit (Qiagen) and cDNA was synthesized using the RevertAid First Strand cDNA Synthesis Kit (ThermoScientific). RNA and cDNA concentrations and quality were determined using a NanoDrop (ThermoScientific). TaqMan Gene Expression Assays (ThermoFisher Scientific)

were used to quantify mRNA expression of *Gnat2*, *Hprt*, and *Rho* (Mm00492394_m1, Mm03024075_m1, and Mm01184405_m1 respectively) (UC Davis Real-Time PCR Research and Diagnostics Core Facility). Relative expression of *Gnat2* and *Rhodopsin* were calculated using the comparative C_T method (also known as the $2^{-\Delta\Delta CT}$ method; Schmittgen and Livak, 2008). This calculation assumes that the PCR efficiency for all genes is similar, which was confirmed for these probes and conditions using multiple dilutions (not shown). Some *Gnat2*$^{-/-}$ samples did not reach C_T threshold for detection within the range of the apparatus although the wells were replicating; in such instances, the samples were assigned the maximum hypothetical C_T value of 40 (based on the cycling conditions) for relative gene expression calculations. Statistical significance was calculated after combining the comparative C_T calculations across independent experiments at a matching dilution using a two-tailed Student's *t*-Test.

2.3. Immunohistochemistry

Mice 6 and 9 months of age were sacrificed by carbon dioxide euthanasia before enucleation. Eyes were fixed in 4% paraformaldehyde for 25–30 min, and the cornea and lens were removed during fixation. To examine histology and protein localization, fixed eyecups were embedded in agarose and sliced into 150 μm thick sections on a vibratome (Leica). Sections were blocked in normal goat serum at room temperature, followed by an overnight incubation with primary antibodies at 4 °C, and then incubation with secondary antibodies for 1.5–2 h at room temperature. To examine the number of cone photoreceptors and microglia morphology, retinal flatmounts were prepared rather than retinal slices. In brief, whole retinas were removed from the fixed posterior pole and cut to relax the curvature. Isolated retinas were incubated in 1% Triton X-100 in PBS overnight at 4 °C followed by blocking with normal goat serum for 2 h in a 37 °C water bath. Primary antibody incubation proceeded overnight at 4 °C, followed by incubation in secondary antibodies for 1.5–2 h in a 37 °C water bath. Both retinal sections and flat mounts were mounted on glass slides with Diamond Antifade Mountant (Life Technologies) before imaging. Primary antibodies and nuclei stains used are listed in Table 1, and secondary antibodies were Alexa Fluor-conjugated (Life Technologies) and used at 1:200 or 1:300 dilution. All sections and flat mounts were imaged using a Nikon A1 confocal microscope.

Cone photoreceptor density was assessed in 5 separate areas of each flat-mounted retina: superior, inferior, nasal, temporal, and central. Two squares of 150 μm × 150 μm were randomly chosen within each area of each retina, and cones were manually selected and quantified using a counting function (Nikon NES-Elements). Statistical significance was calculated using a two-tailed Student's *t*-Test.

2.4. Optical coherence tomography

Mice 5 and 9 months of age were anesthetized with isoflurane and the pupils dilated with tropicamide and phenylephrine. High acquisition-speed Fd-OCT (132 nm @ 855 nm broadband light source [Superlum] and CMOS camera [Basler] operating at 100,000 A-scans/s) were used to obtain *in vivo* mouse retinal volumetric data sets as described in Zhang et al. (2015). Images were acquired over 1.9 × 1.9 mm retinal area (51 deg FOV; see Zhang et al., 2016). OCT volumes were flattened using a strip-registration algorithm to align

each A-scan in the data set. To measure the thickness of retinal layers, all A-scan intensity profiles were averaged from the flattened OCT volume, and evaluated using the choroid, INL, and GCL as landmarks. The distance from choroid to INL defined the outer retinal thickness and the distance from INL to GCL was defined as inner retinal thickness.

2.5. Corneal electroretinography

After dark adaptation overnight, mice were anesthetized with isoflurane and the pupils dilated with tropicamide and phenylephrine. Electroretinograms (ERGs) were recorded with a Maxwellian-view Ganzfeld ERG system (Phoenix Research Labs), equipped with two independent calibrated LED sources (365 and 510 nm). A reference electrode was inserted subcutaneously above the eye, and a ground electrode was inserted subcutaneously at the base of the tail. Combined rod and cone photoreceptor function was characterized using 1 ms flashes of 365 and 510 nm light. Assuming an end-on collecting area of 0.87 μm^2 for rods (Lyubarsky et al., 2004) and a collecting area of 1 μm^2 for cones (Daniele et al., 2005), a flash delivering 100 photons μm^{-2} suppresses an average of ~50% of the circulating current of rods (Peinado Allina et al., 2017), but less than 4% of the circulating current of cones (Nikonov et al., 2006). We thus used this flash strength to probe the scotopic ERG in Fig. 4. In order to isolate cone photoreceptor function, a saturating probe flash (1 ms of 365 nm, 1.22×10^6 photons/ μm^2) was delivered on top of a rod-desensitizing background (5 s of 510 nm light, delivering at least 1×10^5 photons μm^{-2} sec^{-1}).

Dark intervals of 20–60 s were interposed between consecutive flashes to ensure complete recovery. These intervals also served to minimize oscillatory potentials that commonly develop over the course of a recording session. To measure a- and b-wave amplitudes, oscillatory potentials were removed prior to analysis by filtering with a 5 ms boxcar filter. A-wave amplitudes were measured from the baseline to the peak of the negative deflection of the unfiltered traces, and b-wave amplitudes were measured from the peak of the unfiltered a-wave to the peak of the filtered, positive-going deflection. All traces were analyzed using IgorPro 7.06 (WaveMetrics). Statistical significance of comparisons between wild-type and *Gnat2*$^{-/-}$ mice was calculated using a two-tailed Student's *t*-Test. Mice used for ERGs were 3–5 months of age.

3. Results

3.1. Loss of Gnat2 expression does not produce cone dysmorphogenesis or retinal degeneration

Gnat2 expression was targeted for disruption by inserting a 7654 base pair deletion spanning exons 2–9 of the *Gnat2* gene through homologous recombination (Fig. 1A; see Methods section 2.1). Successful disruption of gene expression was first confirmed by examining *Gnat2* mRNA expression levels using quantitative real-time PCR (qRT-PCR). Gene expression was quantified using the comparative C_T method, using *Hprt* as a reference gene. *Gnat2* expression was undetectable; based on our detection limits, mRNA levels were decreased at least 6×10^4-fold in the knock-out retinas (p-value = 0.00055, Fig. 1B). Using the same analysis methods and different primers (see Methods), rhodopsin (*Rho*) expression was likewise quantified and found to be unchanged between *Gnat2*$^{-/-}$ and WT control

littermates (p-value = 0.75, Fig. 1C), consistent with normal rod photoreceptor number and outer segment rhodopsin densities in the mutant retina.

To examine Gnat2 protein expression as well as cone photoreceptor morphology, we used immunohistochemistry and peanut agglutinin (PNA) staining of cones in retinas of both knockout and wild-type littermates (Fig. 2). Staining with PNA revealed comparable outer segment and synaptic morphologies of cones from both genotypes (Fig. 2A). Cone synapses were never observed to be displaced to the inner or outer nuclear layers, and there were no morphological abnormalities observed in the outer plexiform layer. While there was clear Gnat2 immunoreactivity in the cone outer segments of wild-type retinas, there was no detectable staining in the $Gnat2^{-/-}$ retinas, consistent with complete loss of protein expression (Fig. 2A). DAPI staining revealed normal nuclear layers in $Gnat2^{-/-}$ retinas. Indeed, the outer nuclear layers of knock-out mice and wild-type litter mate controls were indistinguishable at 6 and 9 months (ONL thickness measurements, in µm: 6-month-old WT and $Gnat2^{-/-}$, 51.72 ± 5.84 and 52.31 ± 3.87 respectively; 9-month-old $Gnat2^{-/-}$ 53.79 ± 5.63; no statistically significant differences, all p > 0.05). Additionally, staining for both M-opsin (Fig. 2B) and S-opsin (data not shown) was comparable between control and knockout mice, with no evident opsin mislocalization. Finally, the numbers of cones per unit retinal area were counted in retinal flat mounts, with both $Gnat2^{-/-}$ and wild-type littermates showing comparable cell densities (Fig. 2C). Thus, there were no signs of degeneration of cones in the $Gnat2^{-/-}$ mice up to 9 months of age.

Next, we evaluated the thickness and integrity of the retina layers by *in vivo* optical coherence tomography (OCT; Fig. 3A). OCT uses interferometry to extract depth-dependent measures of back-scattered light, and the intensity and axial distribution of this signal are useful means to quantify subtle differences in retinal structure between mice or within an individual animal over time (e.g. Levine et al., 2014; Zhang et al., 2015). OCT B-scans showed the retinal layers in the $Gnat2^{-/-}$ mice to be indistinguishable from those of wild-type mice up to 9 months of age, with all retinas showing clearly delineated nuclear and plexiform layers, transparent (non-scattering) outer nuclear layers as well as an intact external limiting membrane, all signs of healthy photoreceptors (Fig. 3A; Levine et al., 2014). Measurements of outer (Fig. 3B) and inner retina thicknesses (data not shown) revealed no differences between wild-type and knockout strains at any age examined. Thus, there were no overt signs of photoreceptor or retinal degeneration *in vivo*.

To look for more subtle changes in retinal health, we examined the morphology and localization of retinal microglia, the resident macrophages that respond to neuronal injury or stress by changing their morphology and migrating to the site of insult. Staining both retinal sections (data not shown) and flat mounts (Fig. 3C) with the microglial marker Iba1 revealed normal ramified morphologies and normal densities of microglial cells in the outer plexiform layer with no microglial invasion into the nuclear layers. We also examined retinal sections for signs of Müller cell gliosis by immunostaining for GFAP. No difference was detectable between control or knockout retinas (Fig. 3D). These results provide further evidence that degeneration does not occur in the $Gnat2^{-/-}$ retina by 9 months of age.

3.2. Absence of cone-driven retinal signaling in the absence of Gnat2

To assess retinal function in the absence of Gnat2, we used *in vivo* electroretinograms (ERGs). The ERG provides information about the electrical responses of both photoreceptors (the a-wave) and bipolar cells (the b-wave). We first probed rod signaling in dark-adapted animals by recording ERGs in response to a flash that strongly activated rods, but negligibly activated cones (100 photons μm^{-2}; see Methods section 2.5). The ERGs elicited by such a flash were indistinguishable in both amplitude and time course between *Gnat2$^{-/-}$* and wild-type animals (Fig. 4A), suggesting that rod function and rod-driven bipolar cell signaling were normal in *Gnat2$^{-/-}$* mice. Strongly consistent with this hypothesis, intensity-response functions for the a-wave and b-wave amplitudes recorded from dark-adapted animals were indistinguishable between mouse strains (Fig. 4C and D). Moreover, the ERG elicited by a stimulus calculated to saturate both rod and cone responses (1 ms flash of 2×10^6 photons μm^{-2}; Fig. 4B) had nearly identical saturating a-wave amplitudes (WT: 1035 ± 55 μV, mean $\pm$ SEM, n = 5 and *Gnat2$^{-/-}$*: 985 ± 25 μV, n = 3; p-value = 0.462207), consistent with the scotopic a-wave being dominated by rods. The completely normal characteristics of scotopic ERGs of the *Gnat2$^{-/-}$* mice reveal that rod function is unperturbed by the loss of Gnat2 expression in cones.

In contrast, cone-driven ERGs were undetectable in the absence of *Gnat2* expression. In wild-type mice, a bright flash delivered in the presence of a rod-saturating background elicited a photopic ERG response with a cone-driven a-wave of approximately 60 μV in amplitude, while no such cone-driven a-wave was detectable in *Gnat2$^{-/-}$* mice (Fig. 5A–B). Because *Gnat2$^{-/-}$* mice show normal cone morphology and normal rod function but lack visual transduction in cones, this strain is ideal for dissecting the contributions of rods and cones to the ERG across a range of steady light intensities. To examine the conditions under which cone function is manifest in the ERGs of the wild-type mice, we measured the response to an intense ultraviolet flash (365 nm, 1 ms, 1.22×10^6 photons μm^{-2}) in the presence of a 510 nm backgrounds with intensities ranging over 7 $\log_{10}$ units (Fig. 5). A UV flash was used because it strongly activates the predominant mouse cone opsin, S-opsin, which has a 360 nm λ_{max} (Lyubarsky et al., 1999). In contrast, the 510 nm backgrounds negligibly activate the S-opsin, while strongly suppressing the rod circulating current. In the presence of scotopic and mesopic backgrounds up to 1×10^4 photons μm^2 s^{-1} (~10^4 R*/rod/s), both wild-type and *Gnat2$^{-/-}$* mice showed indistinguishable a-wave amplitudes, consistent with predominance of rod electrical responses in this intensity regime. However, as the background intensity increased above 5×10^4 photons μm^{-2} s^{-1}, *Gnat2$^{-/-}$* mice failed to generate detectable ERG responses, whereas wild-type mice continued to show cone-driven flash responses whose maximal amplitude changed negligibly over a 1000-fold range of backgrounds (Fig. 5, insets). These results establish the absence of phototransduction in *Gnat2$^{-/-}$* cones, while also revealing the level of rod excitation (~10^4 R*/rod/s) at which cones become the predominant source underlying the a-wave.

4. Discussion

Many studies that have attempted to dissect rod and cone contributions to retinal signaling have utilized *Gnat1$^{-/-}$* mice, whose rods are rendered completely insensitive to light by the

loss of the alpha subunit of the rod G protein, transducin (Calvert et al., 2000). In contrast, the use of the analogous disruption in cone phototransduction through genetic deletion of the cone G protein, Gnat2, has been hampered by concurrent rod pathway dysfunction or degeneration (Chang et al., 2006; Jobling et al., 2013), effects that can confound conclusions about rod function. Here we have presented evidence that cone photoreceptors can be rendered insensitive to light by abolishing Gnat2 expression without any loss of cone cell numbers or rod function. Thus, for the first time there is a genetic line of mice lacking cone function but having intact rod circuitry, and thus an opportunity to fully examine to the extent to which rods are capable of signaling under mesopic and photopic conditions. Here we summarize our findings in the context of previous efforts in this realm and then discuss the significance of rod signaling at high light intensities for future work.

4.1. Comparison of Gnat2$^{-/-}$ mice to other common cone-silent mice

The *Gnat2*$^{-/-}$ mouse line characterized here is the first example of complete loss of cone phototransduction without degeneration or other morphological abnormalities that have been observed in other mice with *Gnat2* disruption. For example, in the *Gnat2*$^{c.518A > G}$ mouse, in which a missense mutation results in the misfolding of the protein, distinct retinal remodeling is apparent as early as 3 months of age, despite a normal rod ERG. This remodeling includes disruptions in the outer plexiform and nuclear layers, most notably displaced photoreceptor synapses, horizontal cell processes, and bipolar cell dendrites into the outer nuclear layer. These disruptions then become more pronounced with age, as does Müller cell gliosis, both of which are extensive by 12 months of age (Jobling et al., 2013). Such retinal remodeling, especially the displacement of rod bipolar cells into the outer nuclear layer, suggests that rod primary and secondary pathways in the retina are likely perturbed as early as 3 months of age. Presumably, the worsening of this remodeling contributes to the decrease in the rod ERG with age in *Gnat2*$^{c.518A > G}$ mice.

Another commonly used cone phototransduction-incompetent mouse line is *Gnat2*^{cpfl3}, in which a missense mutation results in an early stop codon in the *Gnat2* gene. In this line, loss of cone function is coincident with outer nuclear layer thinning and outer segment vacuolization by 6 months. This is accompanied by a mild but clearly detectable decrease in rod-mediated ERGs with age (Chang et al., 2006), and it has been shown that the secondary rod pathway is entirely abolished in these mice (Nusinowitz et al., 2007). Thus, while both *Gnat2*$^{c.518A > G}$ and *Gnat2*^{cpfl3} lines have allowed significant research into rod-mediated vision (e.g. Umino et al., 2008; Naarendorp et al., 2010; Pahlberg et al., 2017), their use has the potential to introduce significant confounds, particularly for adult or aging studies.

In contrast, at approximately the same ages, the *Gnat2*$^{-/-}$ mouse line showed no differences in retinal thickness between knockout and wild-type littermates both by OCT and standard histological measures of nuclear layer thickness, nor was there any detectable decrease in rod-mediated ERGs. Additionally, there were no differences between knockout and control retinas in Müller cell gliosis or microglial activation, both markers of retinal dysfunction and photoreceptor loss. Most importantly, loss of Gnat2 expression did not result in any detectable change in cone morphology, cell densities, opsin localizations, or rod-driven a- or b-waves. Taken together, these results suggest the *Gnat2*$^{-/-}$ line is a valuable tool for

isolating rod function under mesopic conditions, such as is needed for work investigating rod secondary and tertiary retinal pathways and for behavioral studies. Future studies that rely on downstream retinal circuitry should also take care to examine more subtle features of cone synapses, such as their electrical coupling and horizontal and bipolar cell processes, to ensure there are not as yet undetected compensatory changes resulting from loss of Gnat2.

4.2. The contribution of rods to the normal murine ERG under mesopic intensities

Rod and cone function can be easily separated and examined at very dim and very bright light levels, respectively. However, the wide middle range of light intensities over which phototransduction drives changes in membrane currents concurrently in both rods and cones creates ambiguity both about the absolute sensitivity of cones, as well as the state of functional adaptation of rods. Some behavioral experiments using the $Gnat2^{cpfl3}$ mouse line (Umino et al., 2008), have concluded that rod signaling becomes negligible at intensities greater than -2.0 log cd m^{-2} or roughly 1 photoisomerizations rod^{-1} s^{-1}. In contrast, more recent work in mouse retinal slices has found the primary rod pathway can function at light levels similar to our results, although this work did not entirely rule out an indirect contribution of cones (Long et al., 2013). Behavioral experiments using the $Gnat2^{cpfl3}$ mouse line have found sustained rod function in the presence of background illumination of 10^3 (Nathan et al., 2006) and even 10^4 photons μm^{-2} s^{-1} (Naarendorp et al., 2010), similar to the upper functional limit of rod a-waves found here (Fig. 5A). Various states of rod degeneration may explain some of the differences between these studies, and lead to underestimating rod contributions. Future studies utilizing the $Gnat2^{-/-}$ mouse should be useful in sorting out these discrepancies.

The $Gnat2^{-/-}$ mouse will likely also be useful for investigating the influence of rod signaling pathways on light adaptation mechanisms in the retina. For example, it has been shown that the cone-driven b-wave increases in amplitude during light adaptation, yet the cause of this increase remains unclear (Alexander et al., 2006; Tanikawa et al., 2004; Garon et al., 2010). Because the $Gnat2^{-/-}$ mouse line does not exhibit observable deficiencies in rod signaling, it could be used to dissect the unique contributions of the rod-pathway to post-photoreceptor light adaptation.

4.3. Gnat2$^{-/-}$ mouse as a model of achromatopsia

Finally, the $Gnat2^{-/-}$ line may also be of interest to the community as a mouse model of achromatopsia, a heterogeneous disorder in which the loss of cone function results in deficits in visual acuity, nystagmus, photophobia, and other clinical symptoms. Indeed, although the most common causative achromatopsia mutations are in the cone cyclic nucleotide-gated channel, some cases of achromatopsia have also been causally linked to mutations in Gnat2 (Kohl et al., 2004). While achromatopsia is defined as a lack of cone function, human achromatopsia patients also exhibit a wide range of rod function, ranging from essentially normal to dramatic deficits (Maguire et al., 2017). Both $Gnat2^{cpfl3}$ and $Gnat2^{c.518A > G}$ have been used as mouse models of achromatopsia, generally as models for achromatopsia cases where secondary deficiencies arise (Chang et al., 2006; Jobling et al., 2013). In contrast, this $Gnat2^{-/-}$ mouse line may be useful in modeling the less severe achromatopsia cases, where rod function remains normal (Maguire et al., 2017; Hansen, 1990), or have normal scotopic

ERGs yet display dramatic deficiencies in other measures of scotopic function, such as fast flicker responses (Hansen, 1990). Thus, the *Gnat2*$^{-/-}$ mouse should be a useful model for identifying where in the rod parallel pathways these specific deficiencies arise.

Acknowledgments

## References

Alexander KR, Raghuram A, Rajagopalan AS. 2006; Cone phototransduction and growth of the ERG b-wave during light adaptation. Vis Res. 46 (22) :3941–3948. DOI: 10.1016/j.visres.2006.04.015 [PubMed: 16750238]

Calvert PD, Krasnoperova NV, Lyubarsky AL, Isayama T, Nicoló M, Kosaras B, Wong G, Gannon KS, Margolskee RF, Sidman RL, Pugh EN Jr, Makino CL, Lem J. 2000; Phototransduction in transgenic mice after targeted deletion of the rod transducing alpha -subunit. Proc Natl Acad Sci Unit States Am. 97 (25) :13913–13918. DOI: 10.1073/pnas.250478897

Chang B, Dacey MS, Hawes NL, Hitchcock PF, Milam AH, Atmaca-Sonmez P, Nusinowitz S, Heckenlively JR. 2006; Cone photoreceptor function loss-3, a novel mouse model of achromatopsia due to a mutation in *Gnat2*. IOVS. 47 (11) :5017–5021. DOI: 10.1167/iovs.05-1468

Daniele LL, Lillo C, Lyubarsky AL, Nikonov SS, Philp N, Mears AJ, Swaroop A, Williams DS, Pugh EN Jr. 2005; Cone-like morphological, molecular, and electrophysiological features of the photoreceptors of the *Nrl* knockout mouse. Invest Ophthalmol Vis Sci. 46 (6) :2156–2167. DOI: 10.1167/iovs.04-1427 [PubMed: 15914637]

Deans MR, Volgyi B, Goodenough DA, Bloomfield SA, Paul DL. 2002; Connexin36 is essential for transmission of rod-mediated visual signals in the mammalian retina. Neuron. 36 (4) :703–712. [PubMed: 12441058]

Garon ML, Rufiange M, Hamilton R, McCulloch DL, Lachapelle P. 2010; Asymmetrical growth of the photopic hill during the light adaptation effect. Doc Ophthalmol. 121 (3) :177–187. DOI: 10.1007/s10633-010-9243-0 [PubMed: 20711798]

Hansen, E. Clinical Aspects of Achromatopsia. Night Vision: Basic, Clinical and Applied Aspects. Hess, RF, Sharpe, LT, Nordby, K, editors. Cambridge University Press; 1990.

Jobling AI, Vessey KA, Waugh M, Mills SA, Fletcher EL. 2013; A naturally occurring mouse model of achromatopsia: characterization of the mutation in cone transducin and subsequent retinal phenotype. IOVS. 54 :3350–3359. DOI: 10.1167/iovs.13-11831

Kohl, S, Jägle, J, Wissinger, B. Achromatopsia. In: Pagon, RA, Adam, MP, Ardinger, HH, editors. GeneReviews® [Internet]. University of Washington; Seattle, Seattle, WA: 2004. 1993–2017. updated 2016Available from: https://www.ncbi.nlm.nih.gov/books/NBK1418/

Levine ES, Zam A, Zhang P, Pechko A, Wang X, FitzGerald P, Pugh EN Jr, Zawadzki RJ, Burns ME. 2014; Rapid light-induced activation of retinal microglia in mice lacking Arrestin-1. Vis Res. 102 :71–79. DOI: 10.1016/j.visres.2014.07.011 [PubMed: 25091460]

Long JH, Arshavsky VY, Burns ME. 2013; Absence of synaptic regulation by phosducin in retinal slices. PLoS One. 8 (12) :e83970. doi: 10.1371/journal.pone.0083970 [PubMed: 24376776]

Lyubarsky AL, Falsini B, Pennesi ME, Valentini P, Pugh EN Jr. 1999; UV- and midwave-sensitive cone-driven retinal responses of the mouse: a possible phenotype for coexpression of cone photopigments. J Neurosci. 19 (1) :442–455. [PubMed: 9870972]

Lyubarsky AL, Daniele LL, Pugh EN Jr. 2004; From candelas to photoisomerizations in the mouse eye by rhodopsin bleaching in situ and the light-rearing dependence of the major components of the mouse ERG. Vis Res. 44 (28) :3235–3251. DOI: 10.1016/j.visres.2004.09.019 [PubMed: 15535992]

Maguire J, Parry NRA, Kremers J, Murray IJ, McKeefry D. 2017; The morphology of human rod ERGs obtained by silent substitution stimulation. Doumenta Ophthalmologica. 134 (1) :11–24. DOI: 10.1007/s10633-017-9571-4

Naarendorp F, Esdaille TM, Banden SM, Andrews-Labenski J, Gross OP, Pugh EN Jr. 2010; Dark light, rod saturation, and the absolute and incremental sensitivity of mouse cone vision. J Neurosci. 30 (37) :12495–12507. DOI: 10.1523/JNEUROSCI.2186-10.2010 [PubMed: 20844144]

Nathan J, Reh R, Ankoudinova I, Ankoudinova G, Chang B, Heckenlively J, Hurley JB. 2006; Scotopic and photopic visual thresholds and spatial and temporal discirimination evaluated by behavior of mice in a water maze. Photochem Photobiol. 82 (6) :1489–1494. DOI: 10.1562/2006-02-27-RA-818 [PubMed: 16683905]

Nikonov SS, Kholodenko R, Lem J, Pugh EN Jr. 2006; Physiological features of the S- and M-come photoreceptors of wild-type mice from single-cell recordings. J Gen Physiol. 127 (4) :359–374. DOI: 10.1085/jgp.200609490 [PubMed: 16567464]

Nusinowitz S, Ridder WH 3rd, Ramirez J. 2007; Temporal response properties of the primary and secondary rod-signaling pathways in normal and Gnat2 mutant mice. Exp Eye Res. 84 (6) :1104–1114. DOI: 10.1016/j.exer.2007.02.009 [PubMed: 17408617]

Pahlberg J, Frederiksen R, Pollock GE, Miyagishima KJ, Sampath AP, Cornwall MC. 2017; Voltage-sensitive conductances increase the sensitivity of rod photoresponses following pigment bleaching. J Physiol. 595 (11) :3459–3469. DOI: 10.1113/JP273398 [PubMed: 28168711]

Pang J, Gao F, Lem J, Bramblett DE, Paul DL, Wu SM. 2010; Direct rod input to cone BCs and direct cone input to rod BCs challenge the traditional view of mammalian BC circuitry. Proc Natl Acad Sci Unit States Am. 107 (1) :395–400. DOI: 10.1073/pnas.0907178107

Peinado Allina G, Fortenbach C, Naarendorp F, Gross OP, Pugh EN Jr, Burns ME. 2017; Bright flash response recovery of mammalian rods in vivo in rate limited by RGS9. J Gen Physiol. 149 (4) :443–454. DOI: 10.1085/jgp.201611692 [PubMed: 28302678]

Schmittgen TD, Livak KJ. 2008; Analyzing real-time PCR data by the comparative C_T method. Nat Protoc. 3 (6) :1101–1108. [PubMed: 18546601]

Strettoi E, Novelli E, Mazzoni F, Barone I, Damiani D. 2010; Complexity of retinal cone bipolar cells. Prog Retin Eye Res. 29 (4) :272–283. DOI: 10.1016/j.preteyeres.2010.03.005 [PubMed: 20362067]

Tanikawa A, Bush RA, Takada Y, Mears AJ, Swaroop A, Sieving PA. 2004; Functional rods are required for photopic ERG amplitude increase during light adaptation: study of $NRL^{-/-}$ and $RHO^{-/-}$ mice. Invest Ophthalmol Vis Sci. 45

Umino Y, Solessio E, Barlow RB. 2008; Speed, spatial, and temporal tuning of rod and cone vision in mouse. J Neurosci. 28 (1) :189–198. DOI: 10.1523/JNEUROSCI.3551-07.2008 [PubMed: 18171936]

Zhang P, Goswami M, Zawadzki RJ, Pugh EN Jr. 2016; The photosensitivity of rhodopsin bleaching and light-induced increases of fundus reflectance in mice measured in vivo with scanning laser ophthalmoscopy. Invest Ophthalmol Vis Sci. 57 (8) :3650–3664. DOI: 10.1167/iovs.16-19393 [PubMed: 27403994]

Zhang P, Zam A, Jian Y, Wang X, Li Y, Lam KS, Burns ME, Sarunic MV, Pugh EN, Zawadzki RJ. 2015; *In vivo* wide-field multispectral scanning laser ophthalmoscopy-optical coherence tomography mouse retina imager: longitudinal imaging of ganglion cells, microglia, and Müller glia, and mapping of the mouse retinal and choroidal vasculature. J Biomed Optic. 20 (12) :126005. doi: 10.1117/1.JBO.20.12.126005
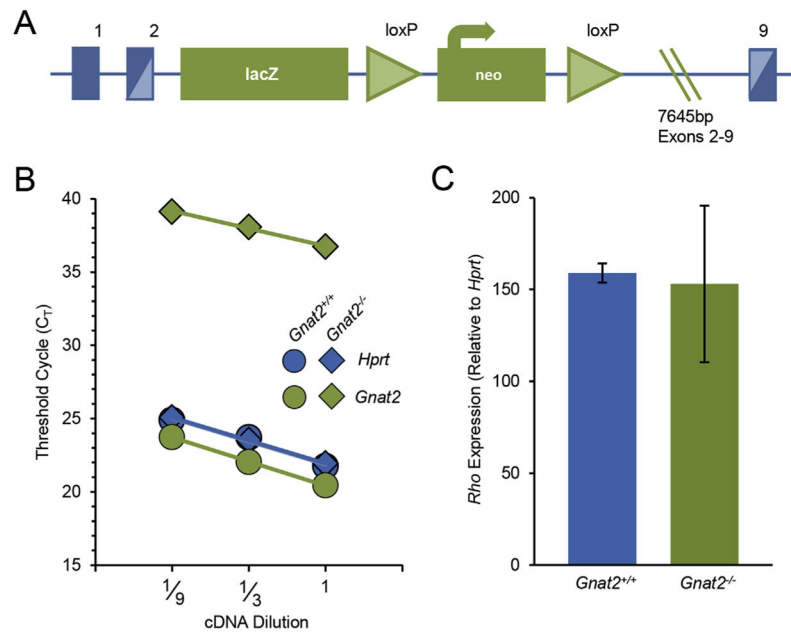
Fig. 1.
Targeted deletion of *Gnat2* decreases *Gnat2* mRNA expression while *Rho* expression remains unchanged. (A) Targeted deletion strategy used to generate the *Gnat2*$^{-/-}$ mouse line (adapted from KOMP). (B) Representative qRT-PCR results from wild-type (filled circles) and *Gnat2*$^{-/-}$ (filled diamonds) littermates 3 months of age. Threshold cycle (C_T) values are shown as a function of cDNA dilutions used for *Gnat2* (green filled) and *Hprt* (blue filled). Across 4 independent experiments, the C_T values for Gnat2 in the knockout were dramatically increased, indicating that there was at least a 60,000-fold reduction in expression in the knockout (p-value < 0.001). (C) Relative rhodopsin expression was unchanged between the knockout and control littermate (p-value = 0.75; *n* = 4–7). Bar graph shows mean $2^{-\Delta C_T} \pm$ SD.
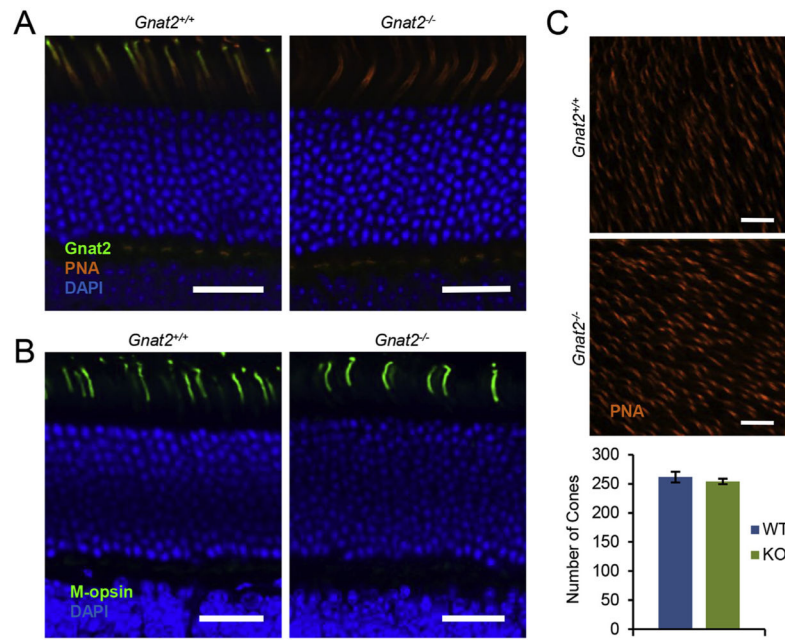
Fig. 2.

Normal cone photoreceptor morphology and number in *Gnat2⁻/⁻* retinas. (A) In retinal sections, PNA staining (orange) showed normal cone morphology and Gnat2 staining (green) confirmed loss of Gnat2 protein in the knockout. Shown here are representative wild-type and *Gnat2⁻/⁻* littermates, 5 months of age. (B) M-opsin staining (green) was the same in wild-type and knockout littermates. (C) Representative 150 μm × 150 μm areas of control and knockout littermate retinal flat mounts stained with PNA to visualize cones. Quantification revealed no difference in the number of cones per unit area (p-value = 0.4817; n = 5 measurements per flatmount, 4 flatmounts from each strain). All scale bars are 25 μm.
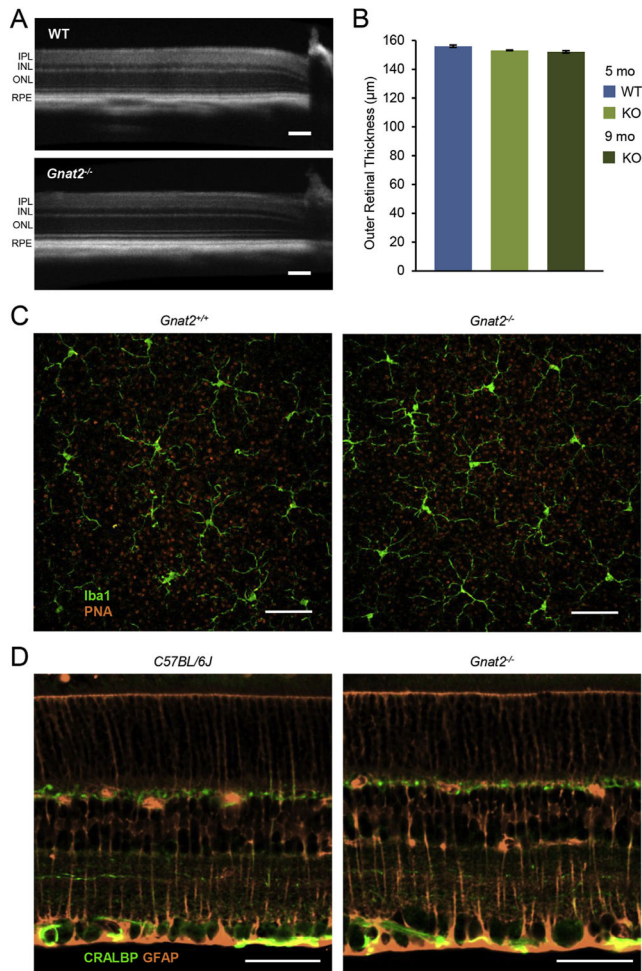
Fig. 3.

Gnat2$^{-/-}$ retinas do not exhibit retinal degeneration. (A) OCT B-scans through the optic nerve head show normal layering of WT and *Gnat2$^{-/-}$* retinas. Shown here are a representative 5-month-old WT retina (top) and a representative 9-month-old *Gnat2$^{-/-}$* retina (bottom). The optic nerve head is located at the far right of each image. Scale bars indicates 100 μm. (B) The outer retinal thickness (choroid to INL) was on average the same in 5-month-old (5 mo) WT and *Gnat2$^{-/-}$* mice, as well as 9 month old (9 mo) *Gnat2$^{-/-}$* mice. Data displayed are mean ± range (n = 4–6 eyes for each). (C) Maximum intensity projections (through 5 μm in z) of the outer plexiform layer of *Gnat2$^{+/+}$* and *Gnat2$^{-/-}$* littermate flat mounts stained for Iba1 (green, microglia) and PNA (orange, cones) reveal normal ramified microglia at the photoreceptor synapses. Scale bars indicate 50 μm. (D) Representative images of retinal sections from C57BL/6J and *Gnat2$^{-/-}$* stained for CRALBP (orange) and GFAP (green) reveal no differences in reactive gliosis. Scale bars indicate 50 μm. IPL, inner plexiform layer; INL, inner nuclear layer; ONL, outer nuclear layer; RPE, retinal pigmented epithelium.
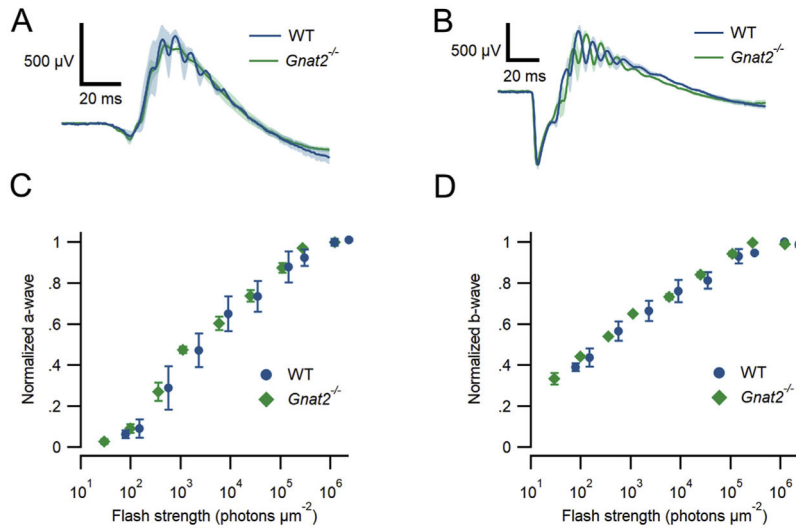
Fig. 4.
Knockout retinas display normal rod-driven a- and b-wave amplitudes. (A) Comparison of the average response of $Gnat2^{-/-}$ (green) and wild-type (WT, blue) animals to a flash of 100 photons μm^{-2}. (B) Average bright flash responses of $Gnat2^{-/-}$ and WT animals (2×10^6 photons μm^{-2}. (C–D) Peak electroretinogram a-wave (C) and b-wave (D) amplitudes of WT (blue circles) and $Gnat2^{-/-}$ (green diamonds) mice in response to increasingly bright flashes of 510 nm light (32–1.22×10^6 photons μm^{-2}).
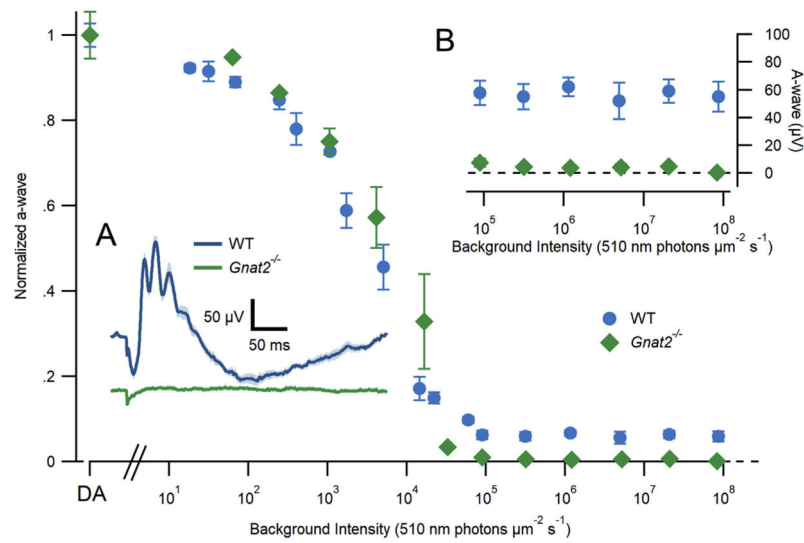
Fig. 5.
Cone-driven ERG responses are absent in *Gnat2*^{−/−} mice. Electroretinogram a-wave amplitudes of WT (blue circles) and *Gnat2*^{−/−} (green diamonds) mice in response to saturating flashes (365 nm; 1.22×10^6 photons μm^{-2}) delivered on increasingly intense 510 nm backgrounds. Insets: (A) Average electroretinogram of WT (blue) and *Gnat2*^{−/−} (green) mice in response to a 1 ms saturating flash delivered on top of a rod-saturating background (510 nm; 1×10^5 photons μm^{-2} s^{-1}). The small deflection in the *Gnat2*^{−/−} trace is an electrical artifact. (B) Expanded view of WT and *Gnat2*^{−/−} a-wave amplitudes at the brightest background intensities. Error bars (frequently smaller than the points themselves) represent SEM.

Table 1

Antibodies and stains used for immunohistochemical staining of retinal sections and flat-mounts.

Target	Host Species or Name	Catalog Number	Manufacturer	RRID	Dilution
Cones	Lectin PNA, Alexa Fluor 568 conjugated	L32458	Life Technologies	NA	1:100
GFAP	Rabbit	Z0334	Dako	AB_10013382	1:1000
Gnat2	Rabbit	LS-C321680	LifeSpan Biosciences	none	1:100
Iba1	Rabbit	019–19741	Wako Pure Chem Industries, Ltd.	AB_2665520	1:1000
M-opsin	Rabbit	None	From Cheryl Craft	AB_2314755	1:100
Nuclei	NucBlue® Fixed Cell Stain	R37606	Life Technologies	NA	1 drop/mL
S-opsin	Rabbit	None	From Cheryl Craft	none	1:100